DØ note 5505
v1.2: November 4, 2007

Search for Excited Electrons in the $ee\gamma$ Channel with the Run IIa Data Set

Volker Vorwerk, Thomas Hebbeker, Arnd Meyer
RWTH Aachen

Abstract

We perform the first search for single excited electron production at the DØ experiment. The electrons are assumed to be produced via contact interactions, leading to an electron and an excited electron: $p\,\bar{p} \to e\,e^* + X$. For the subsequent decay we consider the electromagnetic decay mode $e^* \to e\,\gamma$, resulting in the final state $e\,e\,\gamma$. The analysis is based on data taken at $\sqrt{s} = 1.96\,\mathrm{TeV}$ in Tevatron Run IIa, corresponding to an integrated luminosity of $1013 \pm 61\,\mathrm{pb}^{-1}$.

Since no excess is observed in the data with respect to the Standard Model expectation, upper limits on the excited electron production cross section times branching fraction are derived. These limits correspond to a lower limit of $m_{e^*} > 756\,\mathrm{GeV}$ at 95% CL for a compositeness scale $\Lambda = 1\,\mathrm{TeV}$. We also interpret the result in terms of limits on Λ as a function of m_{e^*}.

1 Introduction

Several models attempt to explain the observation of three families of fundamental fermions, by postulating quarks and leptons to be composed of scalar and spin-1/2 particles. Due to the underlying substructure, compositeness models [1] imply a large spectrum of excited states [1, 2]. Exchange of these substructure particles leads to so called 'contact interactions' (CI) between quarks and leptons [2].

In this analysis, single production of excited electrons via CI is considered, and their subsequent electroweak decay into electron and photon (Fig. 1). This decay mode provides a very characteristic signal, for which the Standard Model (SM) background is small.

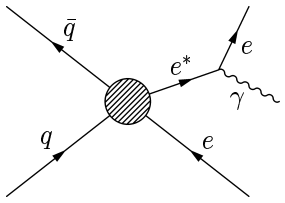

Figure 1: Feynman graph for the process $q\bar{q} \to e^*e \to ee\gamma$.

The gauge particle mediated (GM) production cross section of excited electrons is neglected since it is smaller than 1% of the CI cross section [3]; however, since the acceptance and efficiency for events produced via the two production mechanisms are very similar [4], the current results can easily be interpreted in scenarios where GM interactions dominate.

Decays of excited electrons via CI yield three fermions in the final state - this channel is not selected in the present analysis. The contribution of the CI decays to the total width is significant, however; it is taken into account as a corresponding reduction of the branching fraction of the channel $e^* \to e\,\gamma$, using the BF as given by [2].

The relevant parameters for excited electron production are the excited electron mass m_{e^*} as well as the compositeness scale parameter Λ. Both are important also for the correct description of the decay branching fractions. The parton-level cross section for $e\,e^*$ production via CI is given by [2]:

$$\hat{\sigma}(q\bar{q} \to ee^*) = \frac{\pi}{6\hat{s}} \left(\frac{\hat{s}}{\Lambda^2}\right)^2 \left[1 + \frac{1}{3}\left(\frac{\hat{s} - {m_{e^*}}^2}{\hat{s} + {m_{e^*}}^2}\right)\right] \cdot \left(1 - \frac{{m_{e^*}}^2}{\hat{s}}\right)^2 \left(1 + \frac{{m_{e^*}}^2}{\hat{s}}\right). \quad (1)$$

Here $\hat{s}$ denotes the center of mass energy of the $q\bar{q}$ system. The total width is $\Gamma > 1\,\mathrm{GeV}$ for $m_{e^*} \geq 100\,\mathrm{GeV}$ thus lifetime effects can be neglected in this analysis. We use `Pythia` [5] to simulate excited electron states of this kind.

m_{e^*} [GeV]	σ^{CI}_{prod}(LO)[pb]	BF	σ^{CI}_{prod}(NNLO) × BF[pb]	# events
100	91.8	0.27	34.8	4250
200	24.6	0.21	7.29	5000
300	10.4	0.15	2.22	4250
400	4.37	0.11	0.67	5000
500	2.01	0.082	0.23	3750
600	0.92	0.061	0.078	3750
700	0.31	0.049	0.021	3250
800	0.12	0.037	0.0061	5000
900	0.035	0.031	0.0015	5000
1000	0.010	0.027	0.00037	4500

Table 1: The signal production cross section in LO and in NNLO with $\Lambda = 1\,\text{TeV}$, where the latter includes the effect of a reduced BF to account for CI decays. The same k-factors as for the Drell-Yan process are applied, using m(e^*e) instead of the boson mass.

Typical values of cross sections and branching fractions are shown in Tab. 1, assuming $\Lambda = 1\,\text{TeV}$.

The partial width for the gauge-mediated decay is [2]

$$\Gamma_{GM}\left(e^* \to e\gamma\right) = \frac{1}{8}\,\frac{g_\gamma^2}{4\pi}\,(fT_3 + f'\frac{Y}{2})\,\frac{m_{e^*}^3}{\Lambda^2}\,\left(1 - \frac{m_\gamma^2}{m_{e^*}^2}\right)^2\,\left(2 + \frac{m_\gamma^2}{m_{e^*}^2}\right), \qquad (2)$$

where T_3 is the third component of the weak isospin of the (excited) electron and Y the hyper-charge. The parameters f and f' are determined by the composite dynamics and control the coupling between photons, excited electrons and excited neutrinos. All branching fractions are calculated for the GM decay parameters $f = f' = 1$ [2].

This analysis is based on the diploma thesis of V. Vorwerk [3] and follows the DØ search for excited muons [6, 7]. The current document is an update of DØ Note 5296.

Limits on heavy excited electrons have previously been set at LEP [8], HERA [9], and by CDF [10]. Only the CDF limit is directly comparable to the present analysis because the LEP and HERA results assume production via GM and depend on the relevant couplings. Due to the center-of-mass energy available, the direct lower LEP limits are typically $\sim 200\,\text{GeV}$, and $\sim 250\,\text{GeV}$ for HERA.

2 Monte Carlo Simulation

PYTHIA version 6.313 [5] was used for the signal generation together with the parton density function (PDF) CTEQ6L1 [11, 12]. For simulation of the SM

processes official MC requests generated with PYTHIA version 6.319 and 6.323 were used.

In the detector simulation the effects of multiple interaction are included through the overlay of zero bias events with a luminosity profile similar to the data. The signal Monte Carlo events for the production via CI were produced with the DØ Run II release version p17.09.06. For the SM background, Monte Carlo events were produced with p17.06.02, p17.09.01, and p17.09.06.

The response of the detector is not simulated perfectly in the MC. Correction factors for electrons

$$\epsilon_{corr} = \frac{\text{efficiency}_{\text{data}}}{\text{efficiency}_{\text{MC}}} \tag{3}$$

are applied to tune the simulation. They have been obtained using the tag-and-probe method [13] and are provided by a CAF processor [14]. An example is shown in Fig. 2 (a) in dependency of η. Similar correction factors for photons (Fig. 2 (b)) are described later.

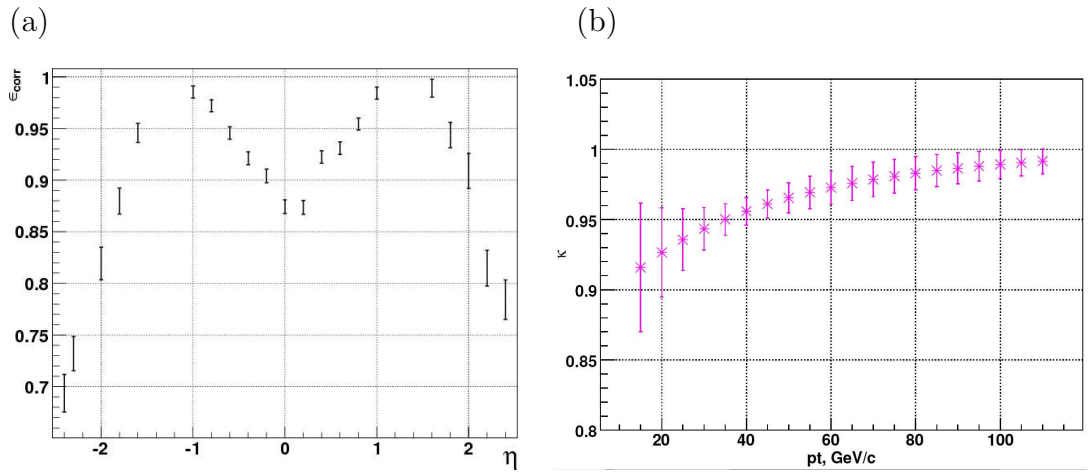

Figure 2: Correction factors for (left) electrons ϵ_{corr} in dependency of η and for (right) photons in dependency of p_T [15] for CC.

2.1 Standard Model Background Processes

2.1.1 $Z/\gamma^* \rightarrow ee$ Drell-Yan Channel

The main background contribution is expected to come from the Drell-Yan process where an additional photon is radiated (ISR or FSR). In Tab. 2 the leading order (LO) cross sections σ_{LO} are listed for $Z/\gamma^* \rightarrow ee$ for different invariant masses of the produced boson. The given cross sections include the BF for the decay into an electron-positron pair (BF$(Z/\gamma^* \rightarrow ee) = 0.0336$ at the Z reso-

nance) [16]. In the right column the numbers of generated inclusive[1] Drell-Yan events are listed.

Z/γ^* mass [GeV]	σ(LO) $\times$ BF [pb]	Request ID (data set)	# events
$15-60$	336	CSG_CAF-MCv2-25012	
		CSG_CAF-MCv2-25013	
		CSG_CAF-MCv2-25014	
		CSG_CAF_MCv3-40668	
		$\vdots$	
		CSG_CAF_MCv3-40677	2221638
$60-130$	181	CSG_CAF_MCv2-26511	
		CSG_CAF_MCv2-26512	
		CSG_CAF_MCv2-26513	
		CSG_CAF_MCv2-26514	
		CSG_CAF_MCv3-30034	
		CSG_CAF_MCv3-30036	
		CSG_CAF_MCv3-30037	
		CSG_CAF_MCv3-30038	
		CSG_CAF_MCv3-38770	
		CSG_CAF_MCv3-38772	
		$\vdots$	
		CSG_CAF_MCv3-38784	
		CSG_CAF_MCv3-34871	
		CSG_CAF_MCv3-34872	
		CSG_CAF_MCv3-34873	4379291
$130-250$	1.37	CSG_CAF_MCv2-24047	
		CSG_CAF_MCv2-24964	207000
$250-500$	0.115	CSG_CAF_MCv2-24052	
		CSG_CAF_MCv2-24967	52750
>500	0.0046	CSG_CAF_MCv2-24262	
		CSG_CAF_MCv2-24970	36000

Table 2: Cross sections for $Z/\gamma^* \to ee$ inclusive in leading order [17].

The k-factors for next-to-next-to-leading order (NNLO) corrections are listed in Tab. 3 and have been multiplied with the LO cross section values [18, 19].

Since the simulated DY process from Pythia does not match the transverse momentum spectrum of the di-lepton system observed in the data, a reweighting was performed [20]. This yields a larger weighting of MC events with high transverse momentum of the Z/γ^* bosons. A high transverse momentum arises

[1]Inclusive means initial and final state radiation are turned on in these samples.

Z/γ^* mass [GeV]	NNLO k-factor	Z/γ^* mass [GeV]	NNLO k-factor
20	$1.23\ ^{+0.06}_{-0.05}$	250	$1.41\ ^{+0.03}_{-0.05}$
30	$1.25\ ^{+0.05}_{-0,05}$	300	$1.41\ ^{+0.04}_{-0.06}$
40	$1.28\ ^{+0.05}_{-0.05}$	400	$1.40\ ^{+0.04}_{-0.07}$
50	$1.30\ ^{+0.05}_{-0.04}$	500	$1.39\ ^{+0.05}_{-0.08}$
75	$1.34\ ^{+0.05}_{-0.04}$	600	$1.38\ ^{+0.05}_{-0.10}$
91.1	$1.36\ ^{+0.05}_{-0.04}$	700	$1.38\ ^{+0.06}_{-0.11}$
100	$1.37\ ^{+0.05}_{-0.04}$	800	$1.37\ ^{+0.07}_{-0.13}$
150	$1.40\ ^{+0.04}_{-0.05}$	900	$1.39\ ^{+0.09}_{-0.15}$
200	$1.42\ ^{+0.03}_{-0.05}$	1000	$1.37\ ^{+0.11}_{-0.17}$

Table 3: NNLO k-factor for the Drell-Yan process. The values as well as the uncertainties are taken from [18].

because the Z boson recoils against jets. Thus, the proportion of jets is expected to increase as well.

Misidentified Photons

If a jet fakes a photon, the final state is the same as for the signal. To estimate the amount of events where a jet fakes a photon, the Drell-Yan MC samples were separated on parton level into events with a 'true' photon and those without. The probability for a jet to be reconstructed as a photon is likely not properly described by the simulation, therefore additional input is needed to correctly estimate the background from Drell-Yan without a genuine hard photon.

We estimate the absolute contribution of jets misidentified as photons in the Drell-Yan sample using the results from the published analysis described in [21]. The probability f_{QCD} for an EM-like jet to be misidentified as a photon is derived as a function of E_T:

$$f_{QCD} = 0.008 + 0.344 \cdot e^{-0.071 \cdot E_T/\mathrm{GeV}}. \tag{4}$$

EM-like jets are selected using the same cuts as for the photon selection (see section 3.2.1), but without applying the final selection criteria on the shower width in the third layer of the EM calorimeter and the isolation in the tracking system. The fake probability f_{QCD} can then be applied to a sample of di-electron events with an additional EM-like jet to obtain the absolute contribution of di-electron plus fake photon events to the di-electron plus photon sample. Details of this procedure are described in [21].

The photon selection criteria in [21] and the present analysis are identical, as well as the definition of EM-like jets.

The absolute normalization of the DY+jet background is applied as a scale factor (~ 2.5) to the DY+jet Monte Carlo. In Fig. 3 the p_T distributions of fake photons estimated from the data are compared with the Monte Carlo prediction. The agreement is good within statistics.

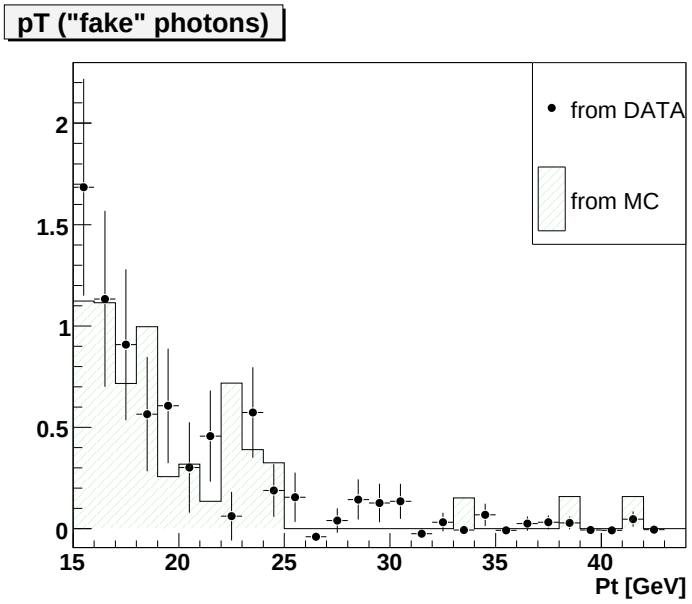

Figure 3: Comparison of the p_T distributions of fake photons in di-electron events determined from data with the Monte Carlo prediction. The black dots show the absolute prediction and shape as obtained from data (see text), while the histogram is the shape predicted from the simulation, normalized to the data.

2.1.2 $Z/\gamma^* \rightarrow \tau\tau$ Drell-Yan Channel

A small contribution originates from the process $Z/\gamma^* \rightarrow \tau\tau$ where the taus decay into electrons, and a photon is radiated (ISR or FSR). The same production cross sections and NNLO corrections as for the $Z/\gamma^* \rightarrow ee$ process are used. 3087300 events have been generated (request ID: CSG_CAF_MCv3-39216 - CSG_CAF_MCv3-39230, CSG_CAF_MCv3-44117, CSG_CAF_MCv3-35711, and CSG_CAF_MCv3-35712).

2.1.3 WW Di-boson Channel

If the two W-bosons decay in the electron channel, the signature can be, together with ISR or FSR of a photon, the same as for the signal process, i.e. $ee\gamma$. But also radiation of a quark or a gluon by one of the initial partons, resulting in a jet, can fake the signature, if the jet was misidentified as a photon.

The NLO cross section for $p\bar{p} \to WW$ is [22]

$$\sigma_{NLO} = \sigma_{LO} \cdot k = 8.14\,\text{pb} \cdot 1.42 = 11.5\,\text{pb}. \tag{5}$$

The NLO correction factors for this process as well as for the WZ production (Sec. 2.1.4) and ZZ production (Sec. 2.1.5) are taken from [22]. For this sample, 200750 events have been generated (request ID: CSG_CAF_MCv3-33682).

2.1.4 WZ Di-boson Channel

The process $q\bar{q} \to WZ$ can lead to an instrumental background. It has the same signature as the signal process, in the case of W and Z decaying in the electron channel and one electron being misidentified as a photon. If no track match is required, photons and electrons are both identified as electromagnetic objects (EM objects).

For this channel, 95500 events were generated (request ID: CSG_CAF_MCv3-30488 and CSG_CAF_MCv3-30488) with a cross section of [22]

$$\sigma_{NLO} = 2.45\,\text{pb} \cdot 1.46 = 3.58\,\text{pb}. \tag{6}$$

2.1.5 ZZ Di-boson Channel

In the case of ZZ production the decay of both bosons into an electron pair is possible. This resembles the signal signature if one electron was not detected and, like in the case of WZ production, one of the three remaining electrons was misidentified as a photon.

102750 Events were generated (request ID: CSG_CAF_MCv3-30486) with a cross section of [22]

$$\sigma_{NLO} = 1.03\,\text{pb} \cdot 1.39 = 1.42\,\text{pb}. \tag{7}$$

2.1.6 $W \to e\nu$ Channel

For the $W \to e\nu$ channel 4543690 events were generated with a cross section [22] of

$$\sigma_{NNLO} = 2580\,\text{pb}. \tag{8}$$

The request IDs are the same as in [17]. The contribution by this channel is found to be negligible. In order for events in this channel to contribute to the final sample, in addition to a (real or fake) photon a misidentified electron would have to be present.

2.1.7 $t\bar{t}$ Channel

Another background is the $t\bar{t}$ channel in the case that both W decay into electrons and an additional photon is radiated. With a cross section of [23]

$$\sigma_{NNLO} = 6.77\,\text{pb}, \tag{9}$$

A total of 597280 events were generated (request ID's CSG_CAF_MCv3-35437, CSG_CAF_MCv3-35438, and CSG_CAF_MCv3-35439).

2.1.8 QCD

QCD background is possible through a process with two (or more) jets and a photon, where the jets are misidentified as electrons. To estimate this background, a QCD sample is extracted from the data using an inverse H-Matrix requirement (see Sec. 3.1).

2.2 The Signal Process

Events for the signal process ($p\bar{p} \rightarrow ee^* \rightarrow ee\gamma$) were generated privately with excited electron masses from 100 GeV up to 1 TeV, in steps of 100 GeV. In Tab. 1 the signal cross section is listed for leading order as well as including NNLO corrections and a decay via GM, i.e. the branching fraction for the e^* decay into photon and electron. The numbers of generated events are listed for each mass. Also the branching fractions BF are listed, which account for the decay $e^* \rightarrow e\gamma$ relative to all possible decay modes, both via GM and CI.

The compositeness scale was chosen to be $\Lambda = 1\,\text{TeV}$. For the NNLO QCD correction the same k-factors as for the Drell-Yan process are used [18, 19]. This is a reasonable assumption because the signal and the Drell-Yan process differ only in their out-going leptons, and follows previous publications [10, 6].

3 Data Sets and Event Selection

Data from Run IIa taken in the years 2002 until early 2006 and corresponding to an integrated luminosity of $1013 \pm 61\,\text{pb}^{-1}$ were analyzed [24, 25] (see Tab. 4).

We use the three following skims which are provided by the common sample group (CSG) [26].

- CSG_CAF_2EMhighpt_PASS3_p17.09.03
- CSG_CAF_2EMhighpt_PASS3_p17.09.06
- CSG_CAF_2EMhighpt_PASS3_p17.09.06b.

At least two electromagnetic objects [27] with a transverse momentum larger than 15 GeV are required. All single [28] and di-electron [29] triggers have been used. The triggers for electromagnetic objects are almost 100% efficient [28, 29].

Runs which are marked as bad for SMT, CFT, calorimeter or muon systems as well as luminosity blocks marked as bad by the Jet/MET group are removed, using the data quality packages dq_defs v2006-11-30 and caf_dq v02-01-01.

Trigger list	Trigger	Good recorded luminosity [pb^{-1}]
V8.0 - V9.0	EM_MX	5.8
V9.0 - V10.0	EM_MX	24.8
V10.0 - V11.0	EM_MX	10.8
V11.0 - V12.0	EM_MX	65.2
V12.0 - V13.0	E1_SH30	232.0
V13.0 - V13.3	E1_SHT22	55.4
V13.3 - V14.0	E1_SHT22	320.1
V14.0 - V15.0	E1_SHT25	333.0
Sum		1047

Table 4: Recorded luminosity used in this analysis, after data quality selection and removal of duplicate events. The specified unprescaled trigger has been used for the calculation of the integrated luminosity in each data taking period. The inefficiency of 3.2% due to the rejection of calorimeter noise is not included in the luminosity numbers in the Table.

Events flagged as containing calorimeter noise (noon noise, ring of fire, coherent noise, and empty crate) are removed by these packages. The use of the calorimeter event quality flags yields an inefficiency of 3.2% [30], compatible with another study in [31].

Duplicate events are removed in data and MC.

3.1 Pre-Selection

At least two electrons are required; they must both fulfill the following certified requirements for tight_hmx_trk [14] electrons:

- |EM-ID| = 10 or 11 ($E_T > 1.5\,\text{GeV}$, $emfrac > 0.9$) and $iso < 0.2$.
  The two objects have to satisfy the requirements for electromagnetic objects [27].
- $|\eta_{det}| < 1.1$ (CC) or $1.5 < |\eta_{det}| < 2.5$ (EC).
- $p_T > 15\,\text{GeV}$ and at least one with $p_T > 25\,\text{GeV}$.
  Both electrons are expected to have high transverse momenta. Since for the signal the leading p_T electron has almost always a transverse momentum larger than 25 GeV, at least one electron is required with $p_T > 25\,\text{GeV}$.
- HMx7 < 12 for CC and HMx8 < 20 for EC.
  The shower shape should be electromagnetic to suppress background from jets.

- $Prob\,(\chi^2_{spatial-trk}) > 0.01$.
  To distinguish between electrons and photons a track match is required.

- $\Delta R > 0.4$.
  The two electrons have to be separated to assure a good reconstruction inside the electromagnetic calorimeter.

- No ECN/ECS combinations.
  For signal events where both electrons are detected in the endcaps, the electrons are almost always in the *same* endcap. Therefore, events with both electrons in *different* endcaps are rejected.

After all pre-selection cuts the number of events in the data sample and the predicted SM background are:

Data: 62930

SM background: $61870 \pm 220\,(stat.) \pm 5680\,(syst.)$

Measurement and theoretical prediction agree well.

Tab. 5 shows the signal efficiency of the cuts for the di-electron event selection, examplarily for a low (300 GeV) and a high (800 GeV) excited electron mass.

	Signal efficiency [%]	
Cut	$m_{e^*} = 300\,\text{GeV}$	$m_{e^*} = 800\,\text{GeV}$
2 EM objects, 2 tracks, $p_T > 15\,\text{GeV}$	44.4	49.0
$HMx7/8 < 12/20$	41.7	45.8
$\Delta R > 0.4$	41.6	45.8
no ECN/ECS	41.1	45.6
$p_T(e1) > 25\,\text{GeV}$	41.1	45.6

Table 5: The cut flow for the signal efficiency is given exemplarily for masses of 300 GeV and 800 GeV. A complete cut flow listing all backgrounds separately can be found in Appendix A

The invariant mass of the two selected electrons is shown in Fig. 4 and Fig. 5. The data were subdivided in three different combinations of regions in the electromagnetic calorimeter where the EM objects were detected, i.e. CC/CC, CC/EC, and EC/EC. One can notice that not only the total number of data and SM background events match well, also the shapes in Fig. 4 and in Fig. 5 (a) show a good agreement for data and SM background, taking into consideration the scaled QCD sample.

To obtain the QCD sample, the shower shape cut for two EM objects was inverted (HMx7 > 12 and HMx8 > 20). In the case that one EM object is not track-matched, it is required to not fulfill the photon-ID cuts (see Sec. 3.2.1).

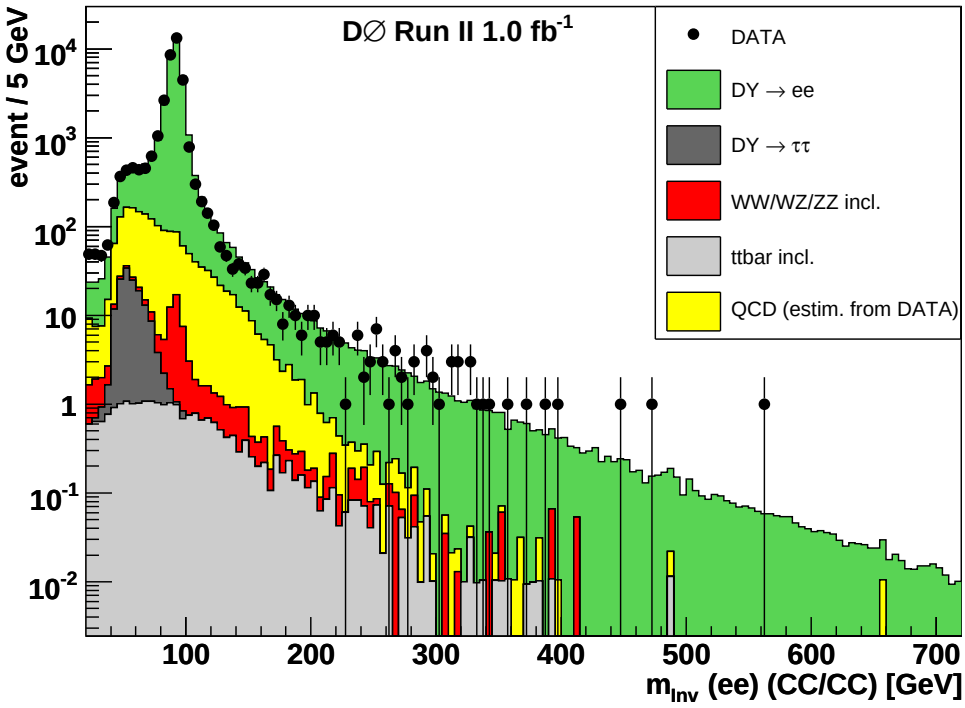

Figure 4: The invariant mass of the two pre-selected electrons for the case that both electrons were detected in the central region of the electromagnetic calorimeter.

This yields a sample orthogonal to the signal selection, and it provides a sample with an invariant mass spectrum shape of mis-identified electrons and genuine QCD background.

We adapted the method to obtain a QCD sample describing the data from [32]: The shape of the QCD sample p_T spectrum was reweighted to match the data. This was done for the leading p_T electron and second electron, and independently for CC and EC. This method is motivated by the fact that EM objects with broader shower shapes (larger H-Matrix) suffer from lower trigger efficiency for lower p_T. Afterwards, the QCD sample was scaled with a global factor, which was obtained from a χ^2-fit, such that the scaled QCD sample and the SM background describe the shape of the di-electron invariant mass distribution of the data. The QCD contribution increases to lower invariant masses. The fit is applied in the lower mass region, from 30 GeV to 65 GeV. In this region, the signal contribution is negligible and is thus not affecting the fit.

The QCD sample is obtained separately for the central and endcap regions, because the shower shape requirements are different for CC (HMx7) and EC (HMx8). Thus, the global fit was performed for the three possible combinations

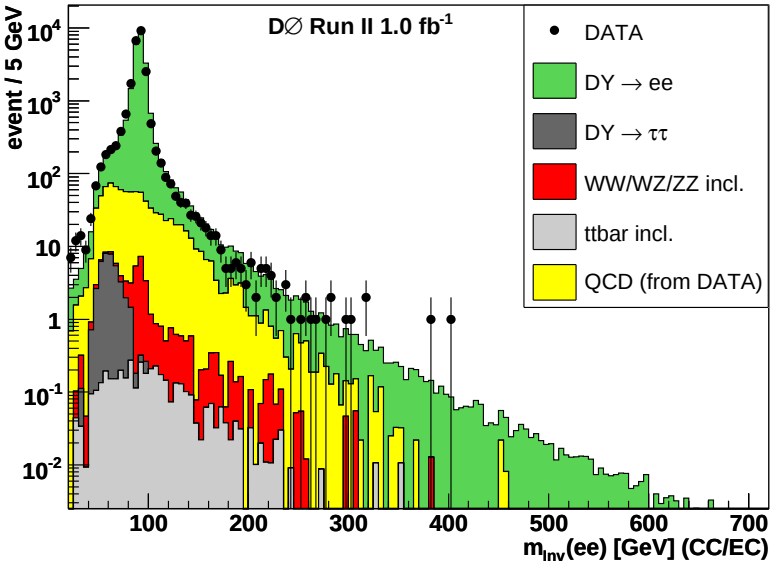

(a)

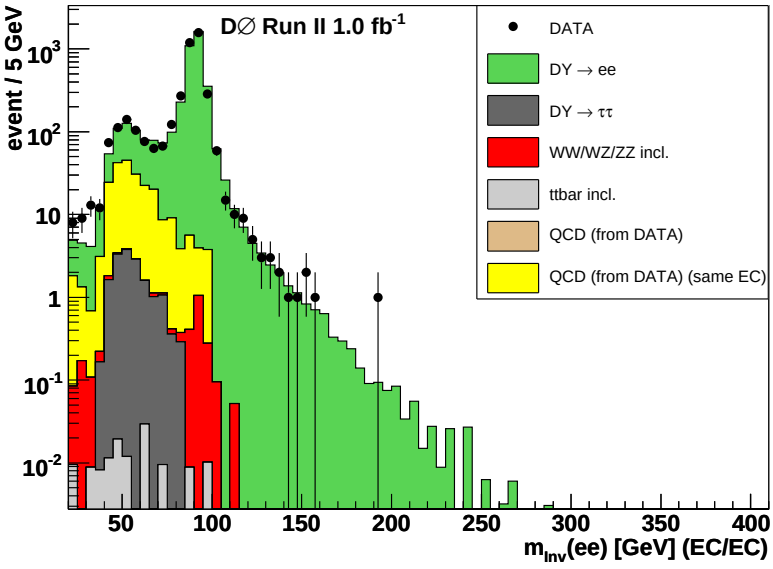

(b)

Figure 5: The invariant mass of the two pre-selected electrons: (a) one electron is detected in the central region, a second electron in the endcap region, (b) both electrons are detected in the same endcap region of the electromagnetic calorimeter.

of detection regions, i.e. CC/CC, CC/EC, and EC/EC.

3.2 Final Sample

From the pre-selection di-electron sample the final sample is obtained by requiring an additional photon.

3.2.1 $ee\gamma$ Selection

Additional requirements for the photon were used as suggested by the photon-ID group [15]:

- Third EM object with $E_T > 15\,\text{GeV}$ and $Prob\,(\chi^2_{spatial-trk}) < 0.001$, with $|\eta_{det}| < 1.1$ or $1.5 < |\eta_{det}| < 2.5$;
- $emfrac > 0.97$;
- $iso < 0.07$;
- in-η-fiducial;
- $\Delta R > 0.4$ between the photon and either of the EM objects;
- (EM cluster width)^2 in $r \times \phi$ and r space:
  $r \times \phi$ width: $\sigma\_\phi\_\text{EM3} < 14\,\text{cm}^2$ for CC,
  $r \times \phi$ width: $\sigma\_\phi\_\text{EM3} < (2.74 \cdot |\eta|^2 - 16.3 \cdot |\eta| + 25.0)\text{cm}^2$ for EC,
  r width: $\sigma\_\text{r}\_\text{EM3} < (5.96 \cdot |\eta|^2 - 30.6 \cdot |\eta| + 40.7)\text{cm}^2$ for EC.
  The width squared ($r \times \phi$ and r) of the EM cluster in the third layer acts as an additional requirement to distinguish between EM objects and QCD background.
- Track isolation.
  The sum of transverse momenta of all tracks within a hollow cone around the photon direction of flight of $0.05 < \Delta R < 0.4$ has to be smaller than $2\,\text{GeV}$.

The cut flow for the $ee\gamma$ selection is shown in Tab. 6. The efficiency is listed for excited electron masses of 300 GeV and 800 GeV. The SM background MC and the QCD background (both included in the column SM BG) describe the data within uncertainties in the final sample:

Data: 259

SM background: $239 \pm 4\,(stat.) \pm 36\,(syst.)$

Cut	SM background [events]	Data [events]	Signal efficiency [%] (300 GeV)	(800 GeV)
3^{rd} EM object ($p_T > 15$ GeV & track veto & CC or EC)	438 + (DY+jet)	601	32.9	36.6
emfrac > 0.97	373 + (DY+jet)	493	32.1	35.2
isolation < 0.07	300 + (DY+jet)	361	31.8	35.1
in-η-fiducial	296 + (DY+jet)	357	31.3	34.5
$\Delta R > 0.4$	295 + (DY+jet)	357	31.3	34.5
σ_ϕ_EM3 & σ_z_EM3	240 + (DY+jet)	259	28.5	33.8
Track isolation	239	259	27.4	32.9

Table 6: Cut flow to obtain the final sample, for the search of an excited electron with a mass of 300 GeV and 800 GeV. For the data and the SM background, the number of events that passed the requirement are listed. The DY+jet contribution due to jets misidentified as photons can only be calculated after applying all photon ID criteria. In the last row, the DY+jet contribution to the total SM expectation is 7 events. For the signal, the efficiency is given. A complete cut flow listing all backgrounds separately can be found in App. A.

The uncertainties are explained in detail in Sec. 4. The different contributions to the SM background are given in the Appendix. About 95% of the SM expectation is due to $DY \to ee$ events with an additional genuine hard photon.

As recommended in [15], exponential functions are used to describe the photon inefficiency that occurs due to the selection requirements; in CC:

$$f^{MC} = 1 - e^{-((1.22)+(0.027)\cdot p_T/\mathrm{GeV})} \quad (10)$$

$$f^{DATA} = 1 - e^{-((0.95)+(0.026)\cdot p_T/\mathrm{GeV})}, \quad (11)$$

and in EC:

$$f^{MC} = 1 - e^{-((0.70)+(0.058)\cdot p_T/\mathrm{GeV})} \quad (12)$$

$$f^{DATA} = 1 - e^{-((0.50)+(0.054)\cdot p_T/\mathrm{GeV})}. \quad (13)$$

Hence, the correction factor for events containing a photon is

$$\epsilon^{\gamma}_{corr} = \frac{f^{DATA}}{f^{MC}}. \quad (14)$$

This scaling factor depends only on the transverse momentum of the photon and varies between 92% and 98% for photon transverse momenta between 15 GeV and 65 GeV (see Fig. 2 b)).

The invariant mass of the final $ee\gamma$ sample is displayed in Fig. 6. The data are described reasonably well by the SM background including the QCD sample. The main SM contribution originates from the Drell-Yan process. For $m(ee\gamma) >$ 200(300) GeV, 19 (3) events are observed in the data, while $14.2 \pm 2.2(2.9 \pm 0.5)$ events are expected from SM processes.

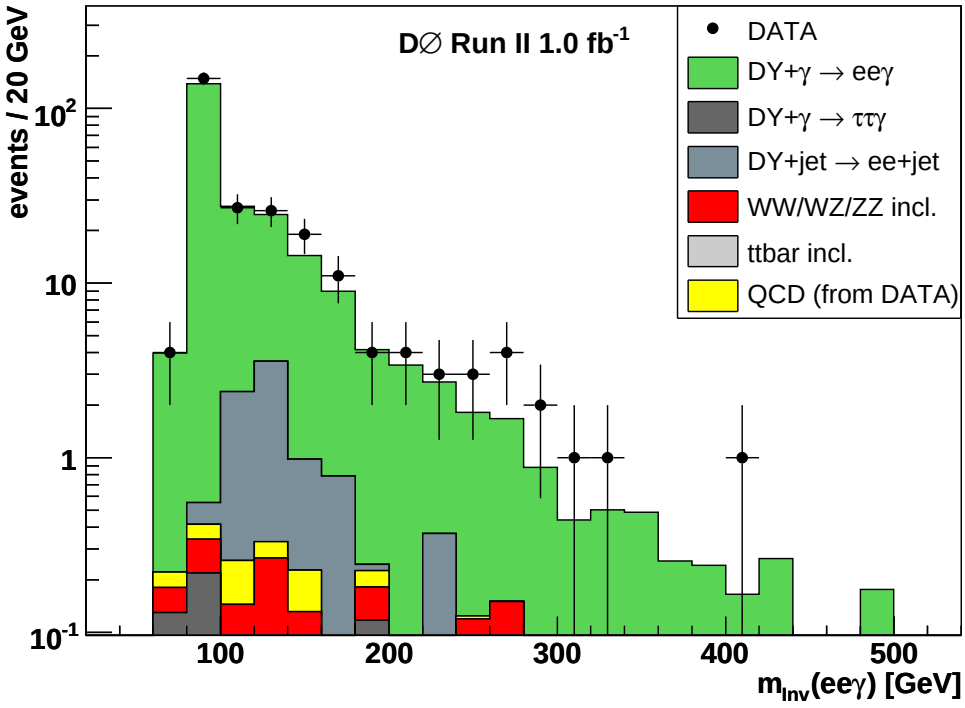

Figure 6: The $ee\gamma$ invariant mass distribution.

Some kinematic quantities are shown in Fig. 7. The transverse momenta of the leading p_T electron, the second electron, and the photon are displayed in Fig. 7 (a,c,e), respectively. Fig. 7 (b,d,f) shows the η distribution of the three final state particles. The photon was identified by the track veto, and it tends to have a lower transverse momentum than the two electrons. In Fig. 8, the separations ΔR between the electrons and the photon are shown. All distributions show a good description of the data by the SM background.

For a better separation of the signal and the SM background, a cut on the invariant mass of the photon and one of the electrons is performed. After such a mass cut, the separation ΔR between the lower p_T electron and the photon allows for low signal masses m_{e^*} a good discrimination of the signal and the SM background. See Sec. 5.1 for the optimization of these final cuts.

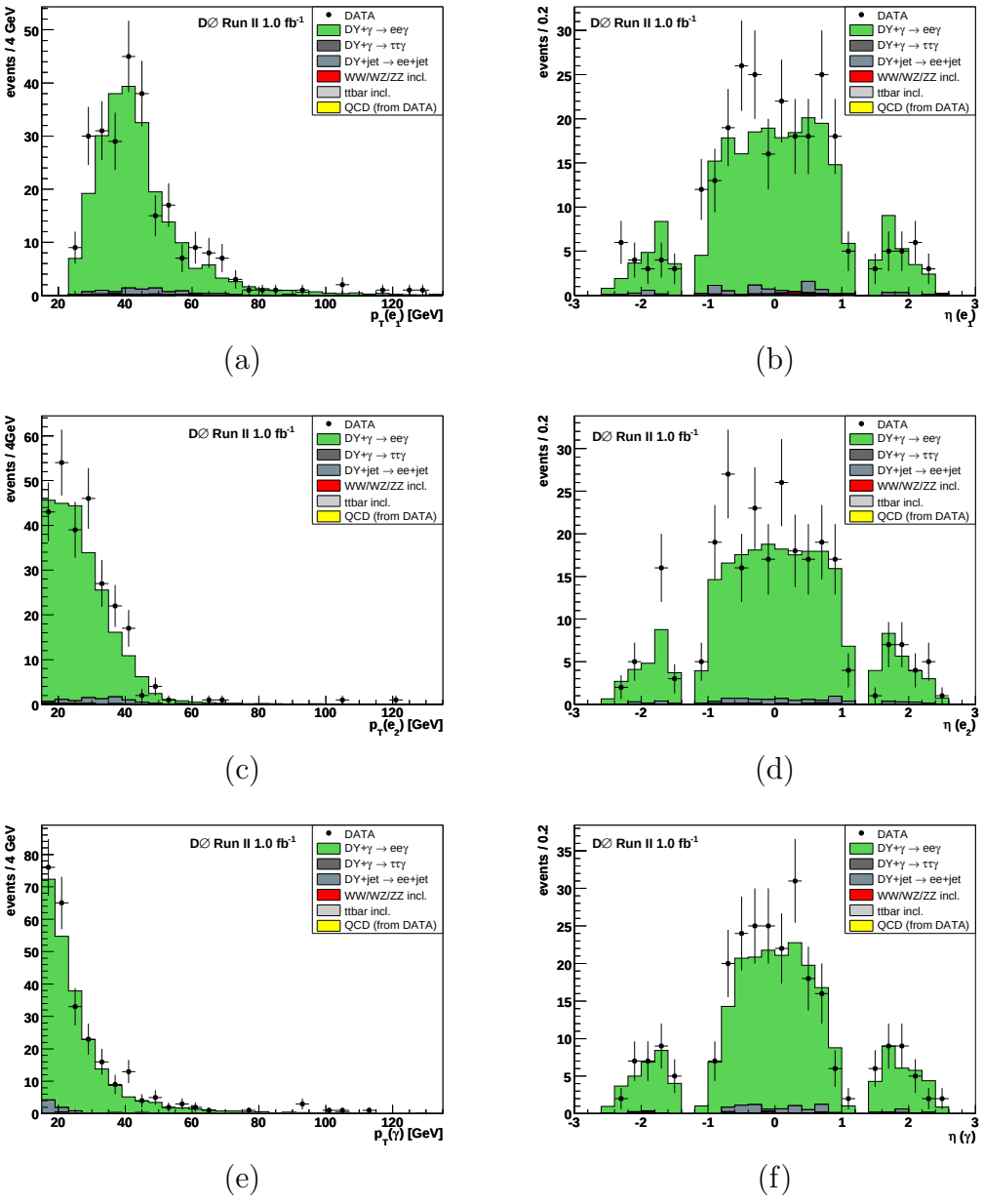

Figure 7: Control plots for the $ee\gamma$ sample. (a) Transverse momenta for the leading p_T electron, (c) for the second electron, and (e) for the photon. In (b) the η distribution of the leading p_T electron is displayed; in (d) and (f) for the second electron and the photon, respectively.

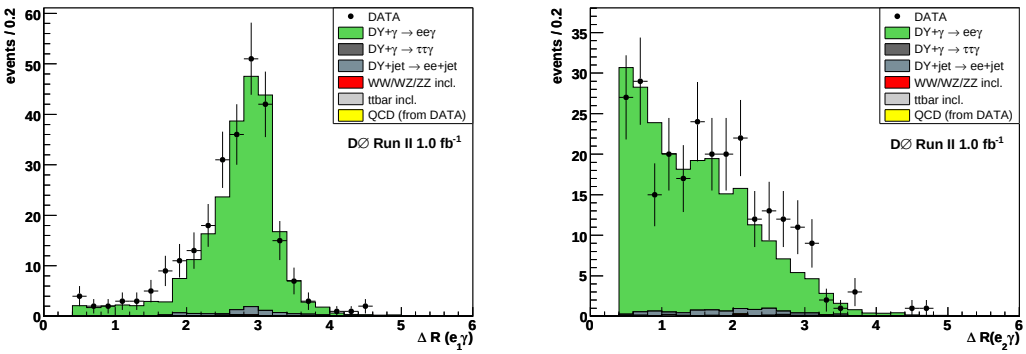

Figure 8: The separation (left) between the leading p_T electron and the photon, and (right) between the second electron and the photon.

4 Systematic Uncertainties

The systematic uncertainties are summarized in Tab. 7 and discussed in the following sections.

Source of uncertainty	Size [%]
EM-ID	2.5 (per electron)
Photon-ID	3.5 (3.7) – 2.0 (1.4) in CC (EC)
Trigger	+0.0 / -3.0
Luminosity	6.1
Higher order corr.	2.8 – 9.9 (for SM cross sections)
QCD background	25 (for this background)
Jet faking photon	60 (for this background)
PDF (acceptance)	1.6 – 6.7

Table 7: List of systematic uncertainties.

4.1 Correction Factors

Electron efficiency correction factors [14] are applied to account for differences between data and MC in the efficiencies of all cut requirements. These factors suffer from uncertainties, where the maximum uncertainty occurs at high $|\eta|$-regions. For the region considered in this analysis, for each electron the maximum uncertainty, 2.5%, is taken as a conservative estimate. In particular the high E_T behavior of the chosen EM-ID cuts has been studied in detail in [17].

For the photon the relative uncertainty due to the correction factor depends on the transverse momentum of the photon [15], e.g. 3.5% (3.7%) for $p_T = 20\,\text{GeV}$ in CC (EC) and 2.0% (1.4%) for $p_T > 30\,\text{GeV}$ in CC (EC) (for CC see Fig. 2).

4.2 Trigger

As mentioned in Sec. 3.1, the triggers are almost 100% efficient [28, 29]. The uncertainties are taken conservatively to be $^{+0\%}_{-3\%}$.

4.3 Luminosity

Also the luminosity calculation is affected by uncertainties. The main contributions originate from uncertainties of the inelastic cross section and the acceptance of the luminosity detector. The sum in quadrature over all contributions yields a total luminosity uncertainty of 6.1% [24, 25].

4.4 Higher Order Corrections

The NLO and NNLO corrections to the Drell-Yan and to the e^* production cross sections are included via the k-factors. Their relative uncertainties are shown in Tab. 8 for the various boson masses and effective center-of-mass energies $\hat{s}$, respectively. The latter are equal to the invariant masses of the excited electron and the associated electron in the case of e^* production.

m_{e^*} [GeV]	k-factor uncertainty [%]
100	3.3
200	2.8
300	3.3
400	3.9
500	4.6
600	5.4
700	6.3
800	7.3
900	8.5
1000	9.9

Table 8: Uncertainties on the total cross section of the Drell-Yan and the signal process due to NLO and NNLO corrections [22].

4.5 QCD Background

The QCD sample was reweighted in the p_T distribution of both objects and then globally with a χ^2-fit to the shape of the di-electron invariant mass distribution for the different regions of the electromagnetic calorimeter (see Sec. 3.1). The statistical uncertainties of the scale factors are negligible compared to the systematic uncertainty of the method by which the QCD sample was obtained. The

latter is estimated by varying the shower shape cut to HMx7/8> 25, in contrast to the default of inverted H-Matrix cuts. This yields a relative uncertainty of 25% on the QCD background estimate. We also investigated the impact of the reweighting procedure on the QCD estimate in the final data sample, and found it to be negligible (about 4% of the QCD background estimate).

4.6 Jets Misidentified as Photons

As a conservative estimate of the photon misidentification rate [21, 33] we use the difference observed between the absolute fake rate prediction from data and simulation. The scale factor is ~ 2.5, therefore the uncertainty estimate is 60%.

4.7 Parton Density Functions

Uncertainties due to the PDFs affect the theoretical production cross sections as well as the efficiency for the signal.

The uncertainty on the signal cross section is considered in the limit calculation (see Sec. 5.2).

The k-factor uncertainties are taken from [18], see Tab.8. These are the same values as for the Drell-Yan process. This is a reasonable assumption because the higher order sub-processes are very similar for both, the production of excited electrons and the Drell-Yan process (compare with [19]).

To determine the uncertainties on the signal efficiency, information delivered by the "pdf_reweighting" processor [34] is used. With this processor the events are reweighted from CTEQ6L (LO) to CTEQ6M (NLO) with respect to their Bjorken-x. For every incoming proton and anti-proton 20 error functions are determined. The efficiency deviation from every of the 20 error functions to CTEQ6M is determined. The quadratical summation of all aberrations yields the efficiency uncertainty for the signal. This efficiency uncertainty for CTEQ6M is now assumed for the generated signal events (CTEQ6L) [35].

The resulting values are 1.6% for $m_{e*} = 100\,\text{GeV}$, 4.3% for $m_{e*} = 500\,\text{GeV}$, and 6.7% for $m_{e*} = 1\,\text{TeV}$. For the other masses the uncertainty was interpolated between these values.

5 Results

After the optimization of the final selection criteria (Section 5.1), the data and the SM prediction agree and no significant excess is observed. Experimental limits are set on the contact interaction production cross section of excited electrons and the subsequent decay into electron and photon. Also for the compositeness scale Λ limits are set.

5.1 Final Sample Selection: $e\gamma$ Invariant Mass

The $ee\gamma$ invariant mass distribution of the final $ee\gamma$ sample is shown in Fig. 9 for two different signal masses, 300 GeV and 800 GeV. The signal is clearly separated from the data and the SM background. No excess in data is observed.

The invariant mass of the hypothetical excited electron can be reconstructed by selecting the photon and one of the electrons (see Fig. 10).

For invariant masses above 200 GeV, out of the two electrons that one is chosen which, when combined with the photon, results in an invariant mass closest to the signal mass searched for. In the case of 100 GeV and 200 GeV the electron with the lower transverse momentum is chosen, which, as has been verified on parton level, is for these masses with high probability the electron from the e^* decay.

The first method causes a certain distortion of the $e\gamma$ invariant mass distribution for both the data and the MC sample (see Fig. 11). As expected, also the background contributions are shifted closer to the hypothetical e^* mass. However, comparing the distributions for different e^* masses one can see that the distortion effect due to this selection is negligible, i.e. does not have a negative impact on the sensitivity, for masses of 300 GeV and above.

Two different methods are compared in order to select the optimal cut region:

1. a symmetrical mass window around the excited electron mass under study;

2. a lower mass cut.

To obtain optimal results, the selection cuts are determined for both methods by comparing the average expected limit. As a result of the comparision, only the second method, using a lower mass cut, is applied (see Tab. 9 for numerical values of the cuts).

We also compared the expected limits with and without rejecting events with both electrons detected in the calorimeter endcaps. The influence of rejecting events with a photon in the EC on the expected limit was investigated, too. For $m_{e^*} > 300$ GeV, where SM backgrounds are very small, all EC electron and photon combinations were kept in order to maximize the acceptance and keep the search as general as possible.

The control plots after these cuts are shown in Fig. 12 (compare Fig. 7), for the case $m_{e^*} = 100$ GeV.

Even after the mass cut, for small excited electron masses the separation ΔR between the electron with lower transverse momentum and the photon is a good quantity to separate signal from background (see Fig. 13). Again, the cut value was optimized to obtain the best expected limit.

The final selection cuts are summarized in Tab. 9.

The selected data and SM background events as well as the signal efficiency after all cuts are listed in Tab. 10. For the SM background expectation and the

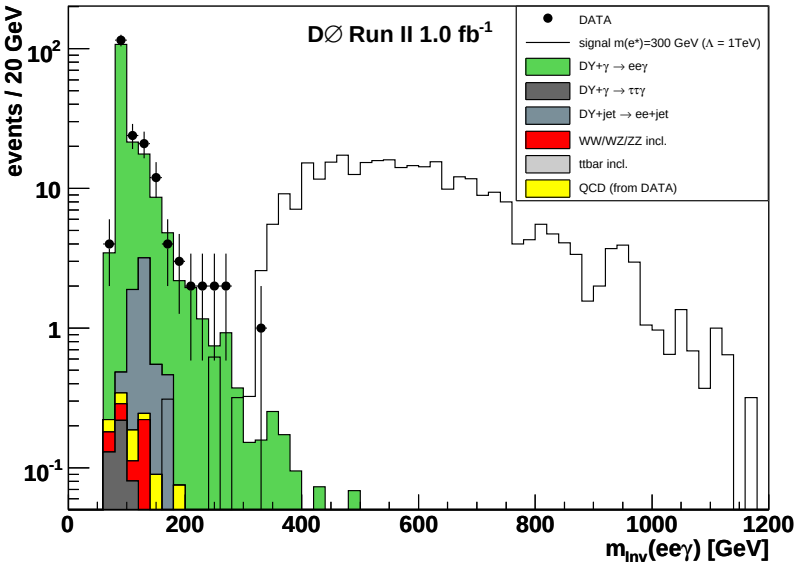

(a)

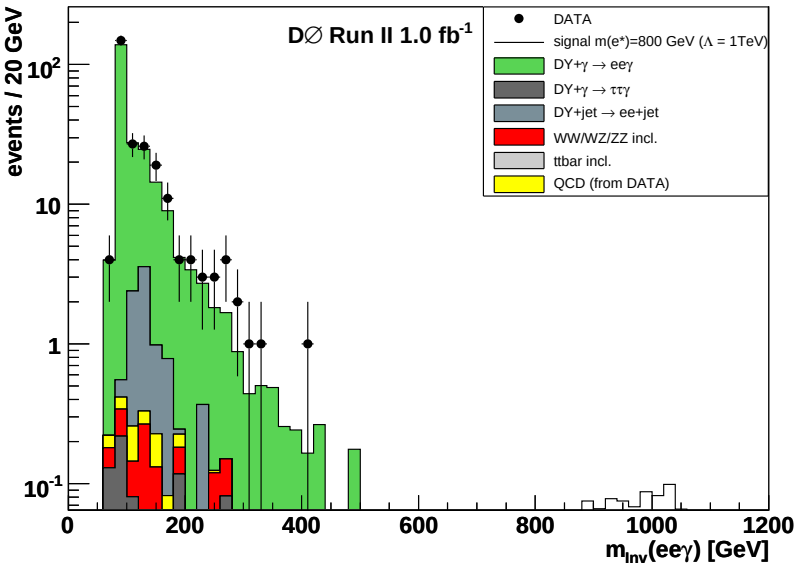

(b)

Figure 9: The invariant mass of the final state $ee\gamma$ for excited electron masses of (a) 300 GeV and (b) 800 GeV. Note that for $m_{e^*} = 300$ GeV events with both electrons and/or the photon in EC are rejected.

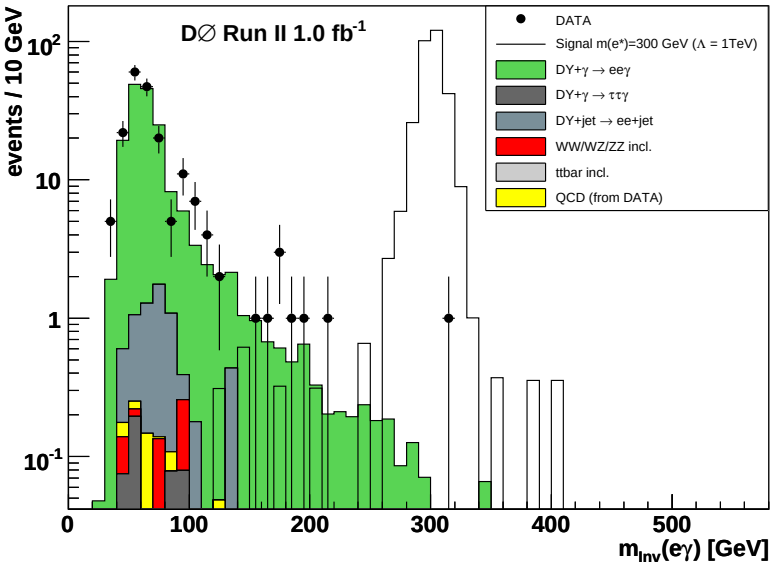

(a)

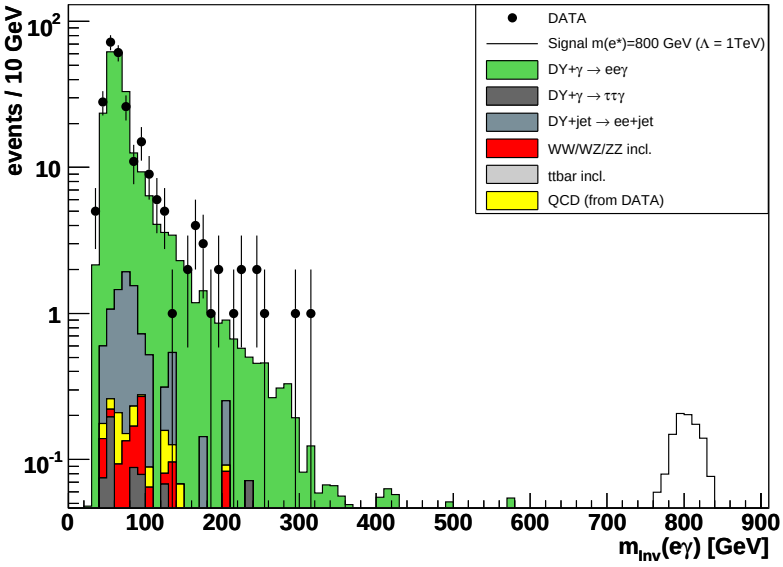

(b)

Figure 10: The invariant mass for the excited electron decay particles e and γ for masses of (a) 300 GeV and (b) 800 GeV. These distributions were obtained by selecting the $e\gamma$ combination closest to the searched e^* mass. Note that for $m_{e^*} = 300\,\text{GeV}$ events with both electrons and/or the photon in EC are rejected.

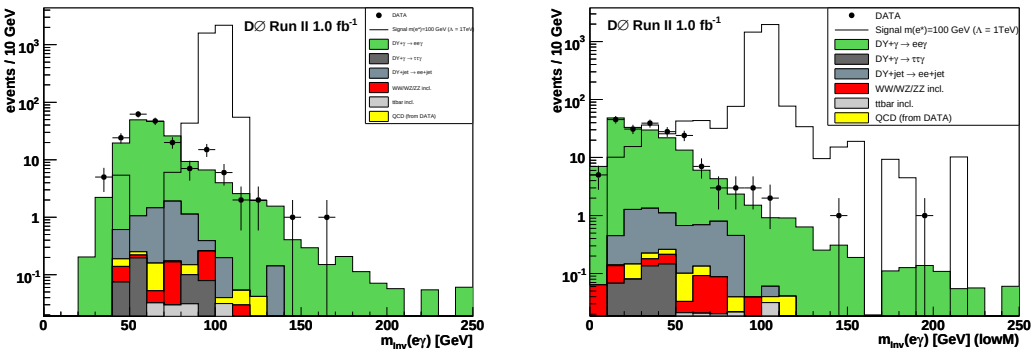

Figure 11: The invariant mass of the excited electron for $m_{e^*} = 100\,\text{GeV}$. The left plot is for the best combination of an electron and the photon, the right one for the combination of the lower p_T electron and the photon.

signal efficiency, statistical and systematic uncertainties are shown. Comparing the event numbers including their uncertainties, no excess is observed. Details for the two remaining data events are given in the Appendix. They appear to be compatible with $Z + \gamma$ production.

5.2 Cross Section Limits

Since no excess is observed in the data, exclusion limits are set. For the production cross section of single excited electrons upper limits are derived, and for the mass, lower limits are set. The limits are calculated using the Bayesian approach and Poisson statistics [36]. The program used ("limit_calculators") is provided by [37].

The results of the limit calculation with 95% confidence level are listed in Tab. 11, as well as the average expected limits. The cross section limits are confronted with theoretical predictions for the e^* production cross section in Figs. 14 (a) and (b).

In Fig. 14 (a), the production cross sections for several values of the compositeness scale ($\Lambda = m_{e^*}$, 1 TeV, 2 TeV, 3 TeV, 4 TeV, 5 TeV) are shown. The theoretical uncertainties on the signal cross section are estimated to 10% (dashed lines in Fig. 14). They have been adopted from Drell-Yan uncertainties [19].

Limits for two different values of Λ are shown in Fig. 14 (b). We determine lower limits on m_{e^*} by comparing the observed cross section limits with the lower boundary of the theoretical expectation. The lower mass limit for excited electrons was determined to

$$m_{e^*} > 756\,\text{GeV} \qquad \text{at } 95\%\ CL$$

assuming $\Lambda = 1\,\text{TeV}$ and $f = f' = 1$. For $\Lambda = m_{e^*}$ with and without BF

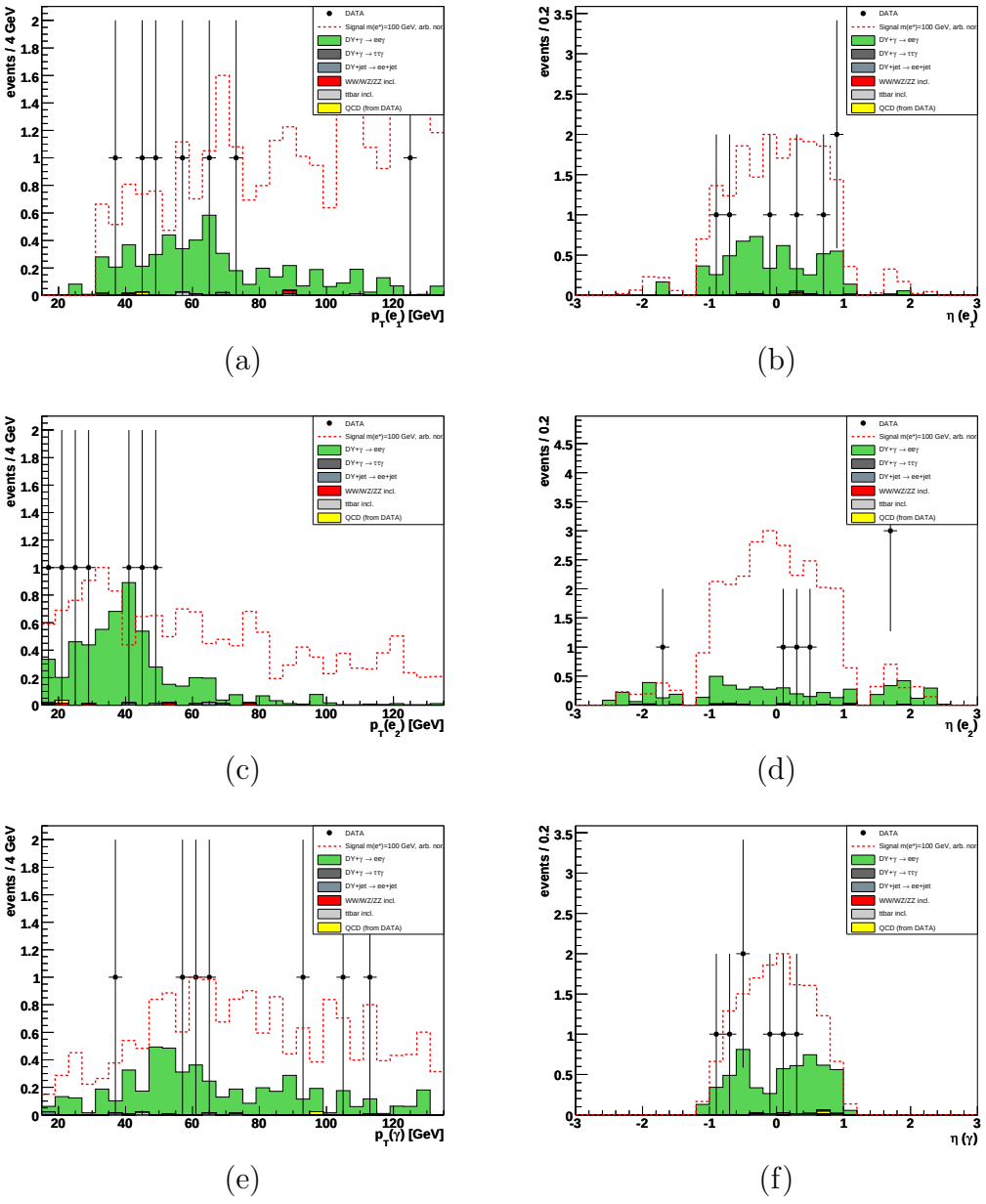

Figure 12: Control plots after all cuts except $\Delta R(e_2, \gamma)$ for the $ee\gamma$ sample and $m_{e^*} = 100\,\text{GeV}$. (a) Transverse momenta for the leading p_T electron, (c) for the second electron, and (e) for the photon. In (b) the η distribution of the leading p_T electron is displayed; in (d) and (f) for the second electron and the photon, respectively. At this stage, 7 events are observed in the data while 5.5 events are expected from SM processes.

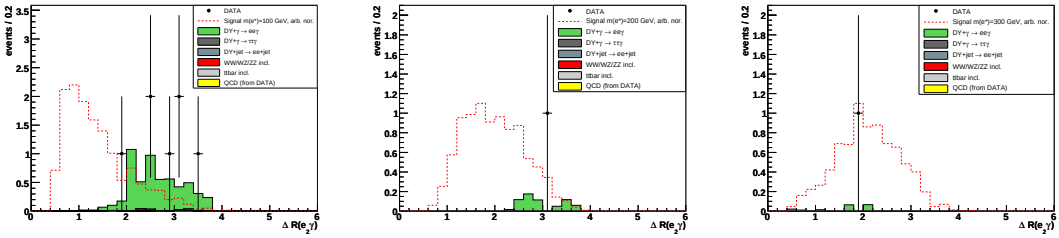

Figure 13: The separation ΔR of the lower p_T electron and the photon after all other cuts for (left) $m_{e^*} = 100\,\text{GeV}$, (middle) 200 GeV, and (right) 300 GeV.

m_{e^*} [GeV]	$m(e_2,\gamma)$[GeV]	$m(e\gamma)^{best}$[GeV]	EC/EC e	EC γ	$\Delta R(e_2,\gamma)$
100	> 90	–	no	no	< 1.8
200	> 165	–	no	no	< 3.3
300	–	> 285	no	no	all
400	–	> 370	yes	yes	all
500	–	> 445	yes	yes	all
600	–	> 515	yes	yes	all
700	–	> 600	yes	yes	all
800	–	> 705	yes	yes	all
900	–	> 800	yes	yes	all
1000	–	> 900	yes	yes	all

Table 9: The selection cuts optimized with respect to the best expected limit. The second and the third columns show the lower mass cuts. The fourth column shows if events with both electrons in EC were rejected, the fifth if events with photons detected in EC are rejected, and the very right one, the upper value for the separation between the second electron and the photon. Events where both electrons were detected in opposite EC's are always rejected.

correction, i.e. consideration of possible decays via CI, the resulting lower mass bounds are 796 GeV and 946 GeV, respectively.

The limits for $\Lambda = m_{e^*}$ with and without BF correction are given to compare the results with recent ones from the CDF Collaboration [10]. In their work, decays via CI were neglected and a compositeness scale of $\Lambda = m_{e^*}$ was chosen. They set a lower mass limit on the excited electron of 879 GeV. Thus the mass bound presented here is the most stringent limit derived so far [2].

If we use the central value of the theoretical signal cross sections for the calculation of the mass limits, the results become $m_{e^*} > 764\,\text{GeV}$ for $\Lambda = 1\,\text{TeV}$; $m_{e^*} > 802\,\text{GeV}$ for $\Lambda = m_{e^*}$; $m_{e^*} > 953\,\text{GeV}$ for $\Lambda = m_{e^*}$ and neglecting CI

[2]In addition, the CDF mass limit was derived with a theoretical cross section too large by a factor of two, due to a bug in older versions of Pythia; later searches for excited muons both by DØ and CDF, as well as the present analysis, have used the corrected cross section.

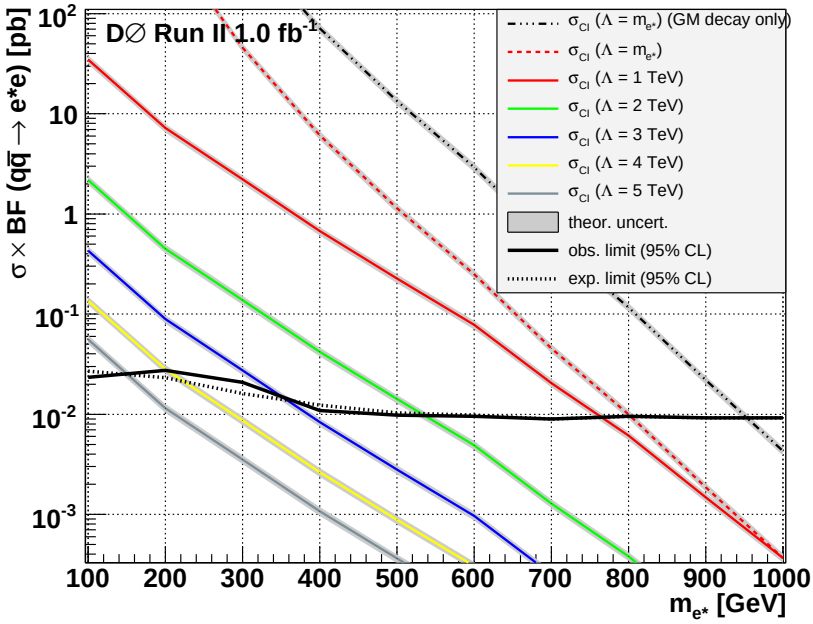

(a)

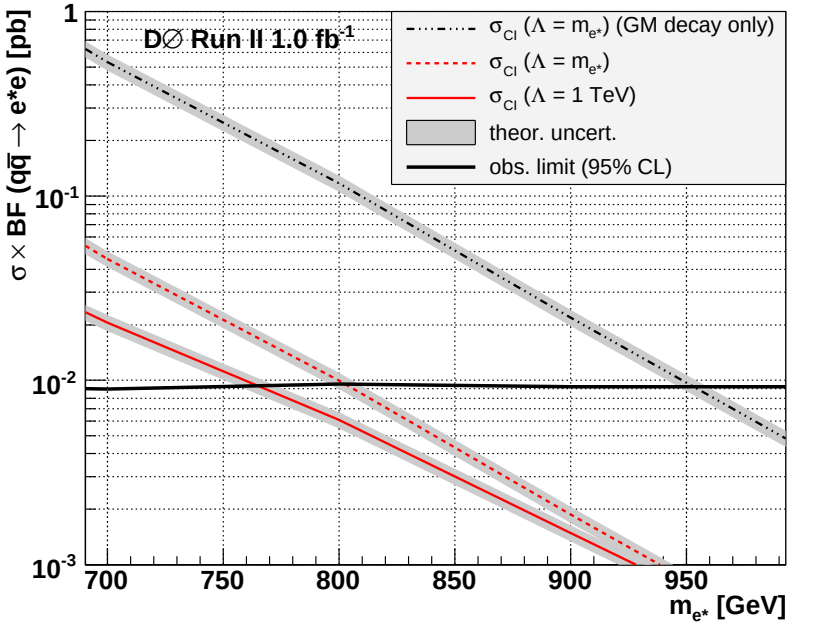

(b)

Figure 14: (a) Limits for the production cross section of single excited electrons. (b) Limits on the production cross section for two different values of the compositeness scale. The limits are at 95% CL.

m_{e^*} [GeV]	Data [events]	SM BG [events]	Signal eff.[%]
100	0	$0.33 \pm 0.09 \pm 0.03$	$13.2 \pm 0.6 \pm 1.3$
200	1	$0.52 \pm 0.16 \pm 0.05$	$16.5 \pm 0.6 \pm 1.6$
300	1	$0.32 \pm 0.12 \pm 0.03$	$22.2 \pm 0.7 \pm 2.2$
400	0	$0.26 \pm 0.11 \pm 0.03$	$28.3 \pm 0.8 \pm 2.8$
500	0	$0.12 \pm 0.08 \pm 0.01$	$31.5 \pm 1.0 \pm 3.1$
600	0	$0.057 \pm 0.054 \pm 0.006$	$32.3 \pm 0.9 \pm 3.2$
700	0	$0.00082 \pm 0.00037 \pm 0.00009$	$34.3 \pm 1.1 \pm 3.4$
800	0	$0.00048 \pm 0.00028 \pm 0.00006$	$32.2 \pm 0.8 \pm 3.2$
900	0	$0.00017 \pm 0.00017 \pm 0.00002$	$33.2 \pm 0.8 \pm 3.3$
1000	0	$0.00017 \pm 0.00017 \pm 0.00003$	$33.3 \pm 0.9 \pm 3.3$

Table 10: Selected data and SM background events for different excited electron mass hypotheses. The efficiency for the signal is listed in the right column. The first uncertainty is always statistical, the second systematic.

decays.

5.3 Limits on the Compositeness Scale Λ

The choice for the compositeness scale $\Lambda = 1\,\text{TeV}$ is quite arbitrary, since the underlying interaction is not known.

The limits on the cross section can be interpreted directly as limits on Λ. Therefore, the lower mass limit for different values of Λ is determined and displayed in Fig. 15.

5.4 Limits within a Gauge Interaction Model

With moderate assumptions, the limits presented here can be interpreted within a model where both production and decay proceed via gauge interactions. From the published CDF results [10, 4], we know that the cross section limits in the GM model are very similar to the CI model – in fact, the GM limits are slightly better. Therefore it is a conservative assumption to use the same acceptance, i.e. the same cross section limits.

Using the GM NNLO cross sections [4, 38] for different e^* masses, we have translated the cross section limits from Tab. 11 into limits on f/Λ within the GM model [2]. The results are summarized in Tab. 12. In Fig. 16, these limits are compared with previously obtained limits by the LEP experiments, H1 and ZEUS, and CDF.

m_{e^*} [GeV]	$\sigma_{\text{prod}}^{\text{observed}} \times BF(e^* \to e\gamma)$ [pb]	$\sigma_{\text{prod}}^{\text{expected}} \times BF(e^* \to e\gamma)$ [pb]
100	0.023	0.027
200	0.027	0.023
300	0.021	0.016
400	0.011	0.012
500	0.0098	0.0103
600	0.0095	0.0098
700	0.0089	0.0089
800	0.0095	0.0095
900	0.0092	0.0092
1000	0.0092	0.0092

Table 11: Upper cross section limits for the production of single excited electrons with 95% CL. The average expected limits are shown in the right column.

m_{e^*} [GeV]	$\sigma^{GM}(NNLO)$ [pb]	f/Λ [GeV^{-1}]
100	3.498	$8.3 \cdot 10^{-4}$
125	0.9534	—
150	0.3827	—
175	0.1844	—
200	0.09920	$2.3 \cdot 10^{-3}$
225	0.05716	—
250	0.03457	—
275	0.02162	—
300	0.01386	$4.1 \cdot 10^{-3}$

Table 12: Upper limits on f/Λ within the GM model for different values of m_{e^*}. Also given are the NNLO cross sections within this model.

Acknowledgments

We would like to thank everybody from the DØ Collaboration who helped with this analysis. We especially appreciate support from C. Autermann, P. Bargassa, J.W. Coenen, S. Desai, J.-F. Grivaz, C. Magass, Y. Maravin, O. Mundal and P. Verdier. We thank Y. Enari, R. Illingworth and S. Fu for saving our data from a disk failure.

A Cut flow for the pre-selection and the final sample

Expected and selected numbers of events are listed in Tab. A.

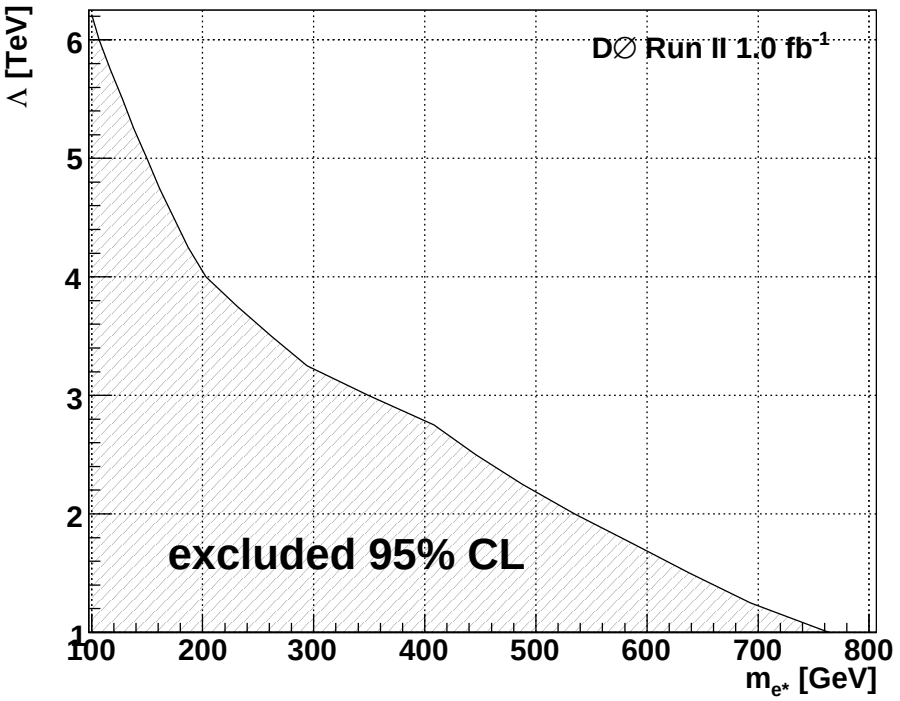

Figure 15: The limit on the compositeness scale Λ at 95% CL as a function of the excited electron mass.

B Candidate Events

At the end of the event selection, two events remain in the data, one each for the hypothetical e^* masses of 200 GeV and 300 GeV, respectively. Details for these events are given in Tab. 14, and event displays are shown in Figs. 17 and 18.

C Mass Spectra with and without QCD Reweighting

See Fig. 19.

References

[1] H. Terazawa, M. Yasue, K. Akama and M. Hayashi, Phys. Lett. B **112**, 387 (1982); F.M. Renard, Il Nuovo Cimento **77 A**, 1 (1983); A. De Rujula, L. Maiani and R. Petronzio, Phys. Lett. B **140**, 253 (1984); E.J. Eichten,

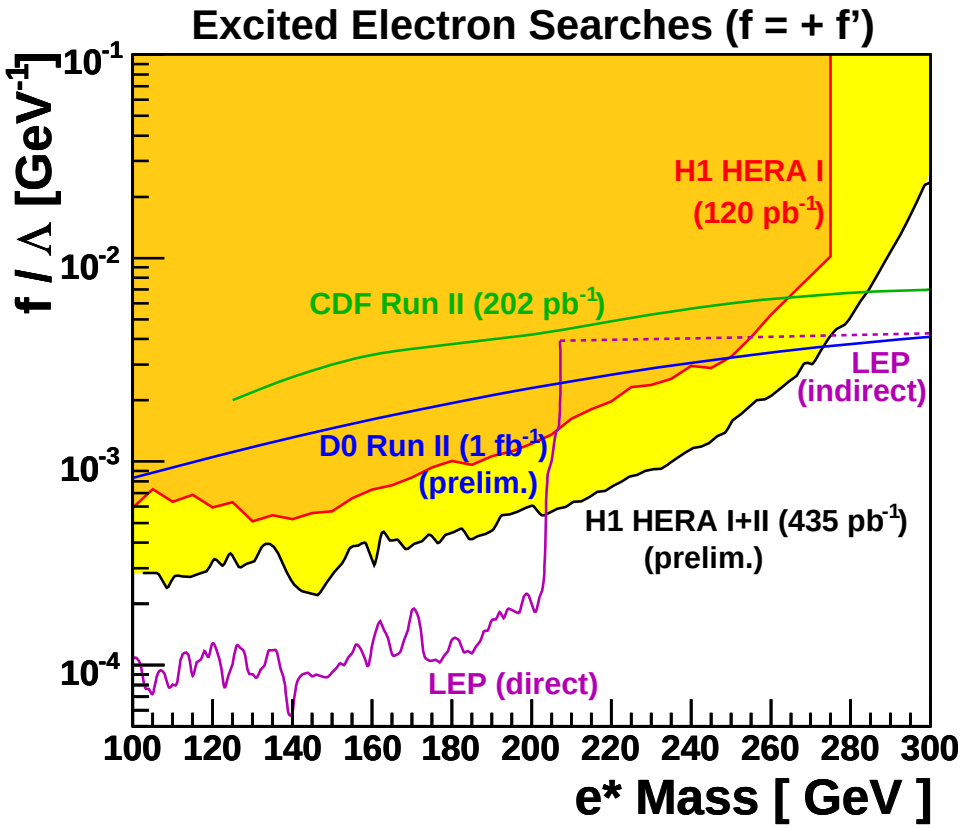

Figure 16: Exclusion limits for GM production and decay of excited electrons obtained by different experiments in the f/Λ versus m_{e^*} plane [39]. The DØ limit is derived under the assumption of the same acceptance for GM production as for the contact interaction model.

K.D. Lane and M.E. Peskin, Phys. Rev. Lett. **50**, 811 (1983); M. A. Shupe, Phys. Lett. B **86**, 87 (1979).

[2] U. Baur, M. Spira and P.M. Zerwas, *Excited Quark and Lepton Production at Hadron Colliders*, Phys. Rev. D **42**, 815 (1990).

[3] V. Vorwerk, *Search for Excited Electrons with the DØ Experiment at the Tevatron Collider*, Diploma Thesis, RWTH Aachen (2006), http:// www.physik.rwth-aachen.de/∼hebbeker/theses/vorwerk_diploma.pdf.

[4] H.K. Gerberich, *Search for Excited or Exotic Electron Production using the Dielectron + Photon Signature at CDF in Run II*, Ph.D. Thesis, Duke University (2004).

[5] T. Sjöstrand *et al.*, Comput. Phys. Commun. **135**, 238 (2001); http://www.thep.lu.se/∼torbjorn/Pythia.html; hep-ph/0308153.

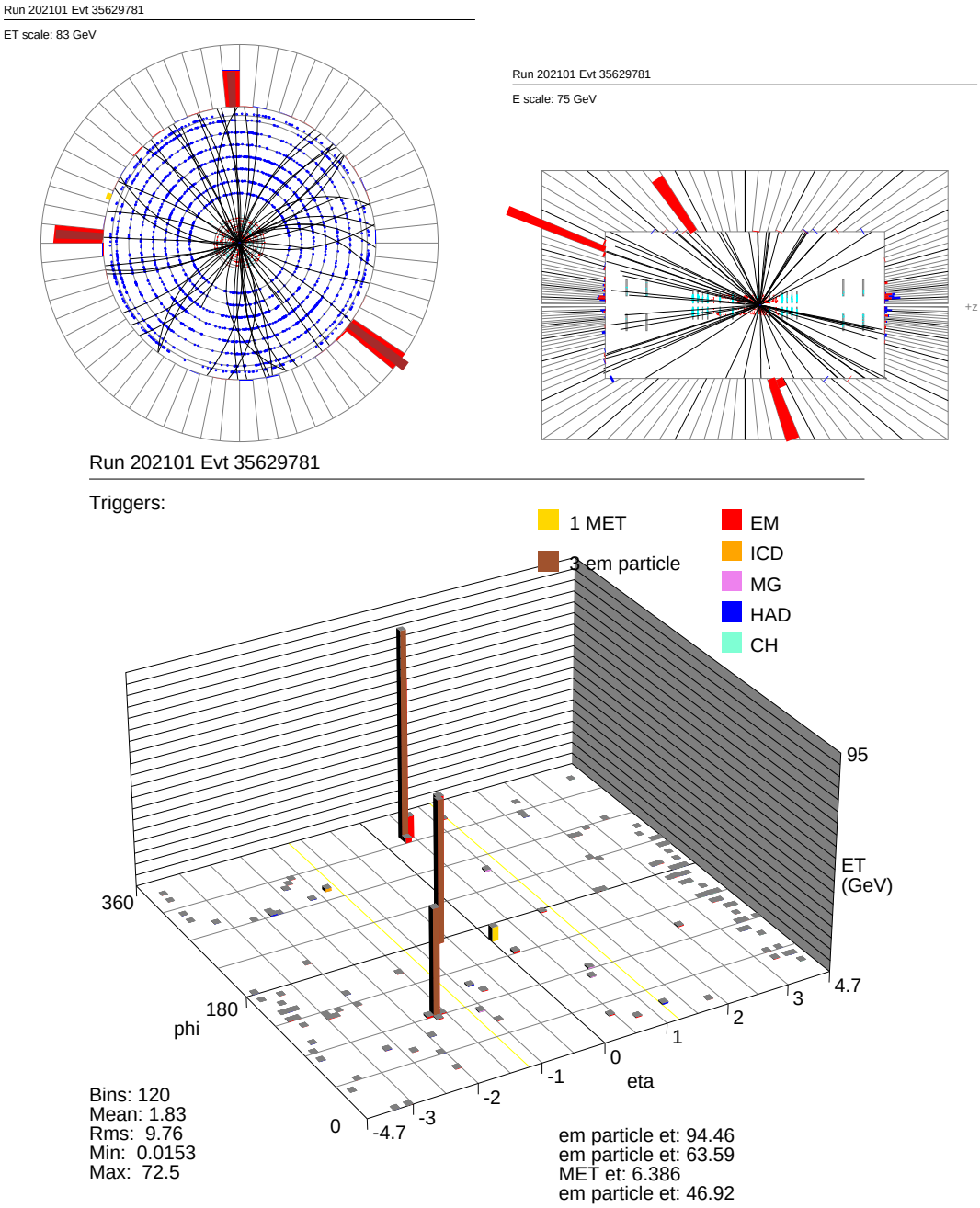

Figure 17: Event display: run number 202101, event number 35629781

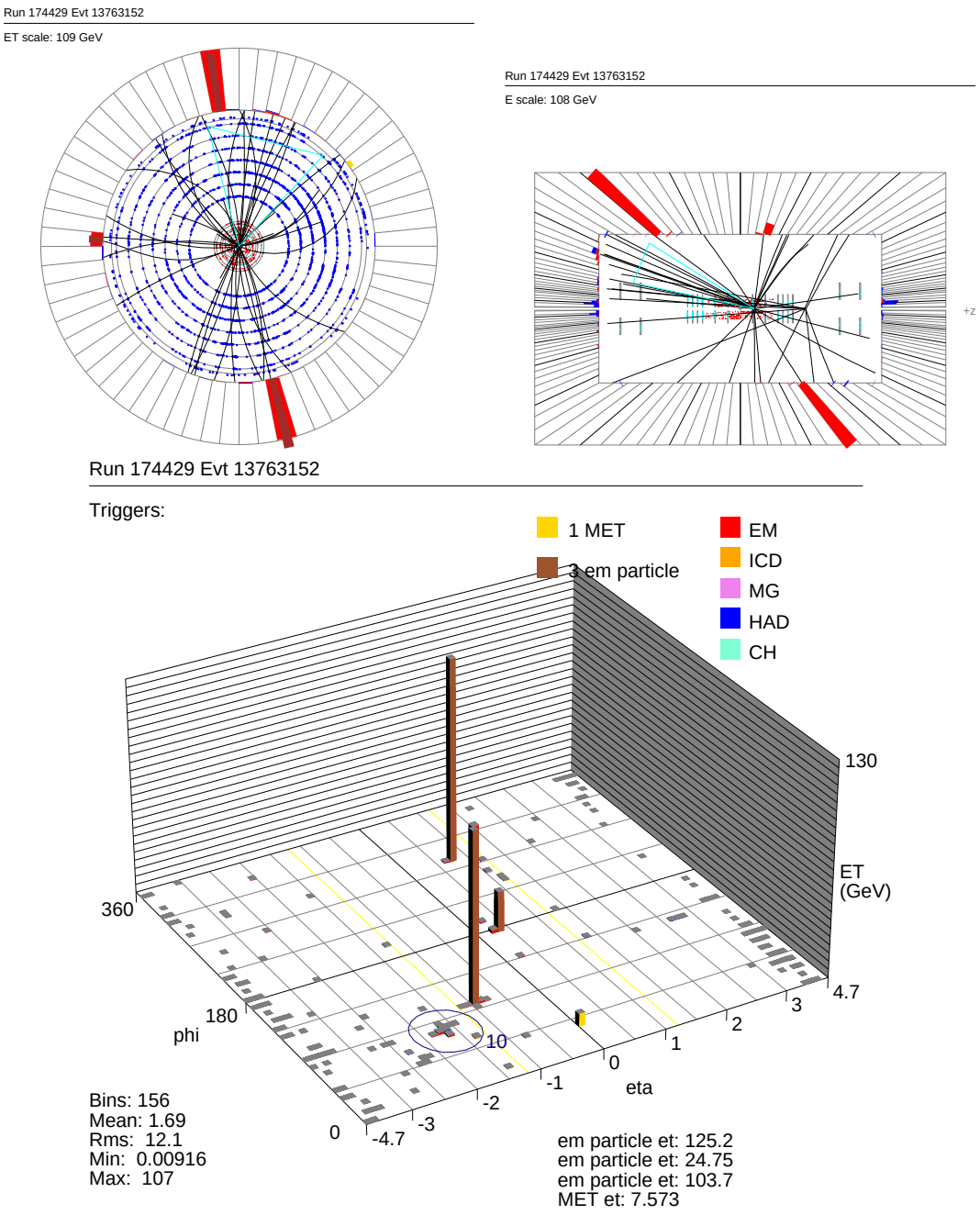

Figure 18: Event display: run number 174428, event number 13763152

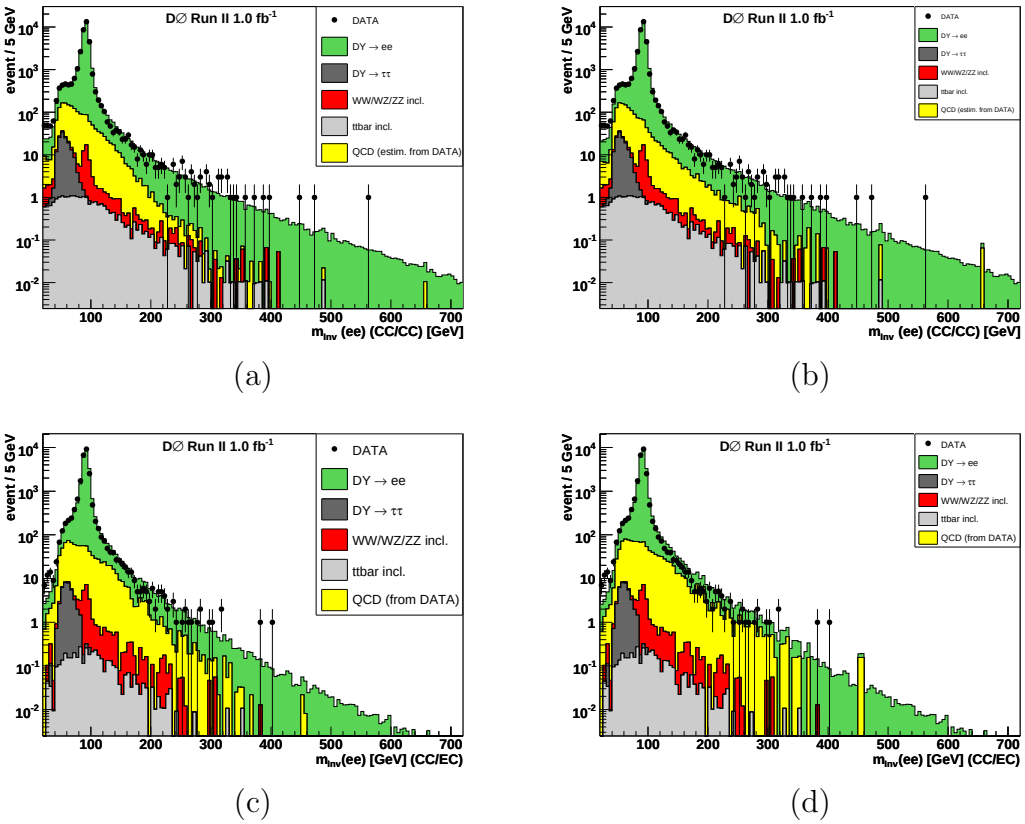

Figure 19: The invariant mass of the two pre-selected electrons: (a) both electrons are detected in the central region, (c) one electron is detected in the central region, a second electron in the endcap region. (b) and (d) show the same distributions but without the QCD reweighting applied.

[6] V.M. Abazov *et al.* (DØ Collaboration), *Search for Excited Muons in $p\bar{p}$ Collisions at $\sqrt{s} = 1.96\,\text{TeV}$*, Phys. Rev. D **73**, 111102 (2006).

[7] J.W. Coenen, *Search for Excited Muons in $p\bar{p}$ Collisions at $\sqrt{s} = 1.96\,\text{TeV}$*, Diploma Thesis, RWTH Aachen (2005), http://www.physik.rwth-aachen.de/∼hebbeker/theses/coenen_diploma.pdf.

[8] G. Abbiendi *et al.* (OPAL Collaboration), Phys. Lett. B **544**, 57 (2002); P. Achard *et al.* (L3 Collaboration), Phys. Lett. **B568**, 23 (2003); J. Abdallah *et al.* (Delphi Collaboration), Eur. Phys. J. **C46**, 277 (2006); R. Barate *et al.* (Aleph Collaboration), Eur. Phys. J. **C4**, 571 (1998).

[9] C. Adloff *et al.* (H1 Collaboration), Phys. Lett. **B548**, 35 (2002); S. Chekanov *et al.* (ZEUS Collaboration), Phys. Lett. **B549**, 32 (2002).

[10] D. Acosta *et al.* (CDF Collaboration), *Search for Excited and Exotic Electrons in the $e\gamma$ Decay Channel in $p\bar{p}$ Collisions at $\sqrt{s} = 1.96\,\text{TeV}$*, Phys. Rev. Lett. **94**, 101802 (2005); hep-ex/0410013.

[11] J. Pumplin *et al.*, *New Generation of Parton Distributions with Uncertainties from Global QCD Analysis*, JHEP **0207**, 012 (2002).

[12] D. Stump *et al.*, *Inclusive Jet Production, Parton Distributions, and the Search for New Physics*, JHEP **0310**, 046 (2003).

[13] J. Hays, J. Mitrevski, C. Schwanenberger and T. Toole, *Single Electron Efficiencies in p17 Data and Monte-Carlo Using p18.05.00 d0correct*, DØ Note 5105 (2006).

[14] The CAF EM-ID Cuts Package, `http://www-d0.fnal.gov/d0dist/dist/packages/emid_cuts/v02-04-07/doc/`.

[15] O. Atramentov, A. Askew, D. Bandurin, D. Duggan, A. Ferapontov, Y. Gershtein, Y. Maravin, G. Pawloski, *Photon Identification in P17 Data*, DØ Note 4976 (2005).

[16] W.-M. Yao *et al.* (Particle Data Group), J. Phys.. G **33**, 1 (2006).

[17] C. Magass, *Search for New Heavy Charged Gauge Bosons Decaying in the Electron Channel*, DØ Note 5190 (2006); DØ Note 5340 (2007).

[18] T. Nunnemann, *NNLO Cross Sections for Drell Yan, Z and W Production using Modern Parton Distribution Functions*, DØ Note 4476 (2004); `http://www-clued0.fnal.gov/∼nunne/cross-sections/dy_cross-sections.html`.

[19] R. Hamberg, W.L. van Neerven and T. Matsuura, *A Complete Calculation of the Order α_s^2 Correction to the Drell-Yan k-factor*, Nucl. Phys. B **359**, 343 (1991).

[20] B. Tiller and T. Nunnemann, *Measurement of the Differential Z^0-boson Production Cross-Section as Function of Transverse Momentum*, DØ Note 4660 (2004); implementation in the caf_mc_util package.

[21] A. Ferapontov and Y. Maravin, *Study of $Z\gamma$ Events in DØ Run II p17 Data*, DØ Note 5156 (2006).

[22] J.M. Campbell and R.K. Ellis, Phys. Rev. D **60**, 113006 (1999); J.M. Campbell and R.K. Ellis, http://mcfm.fnal.gov/; T. Nunnemann, MCFM Cross Sections, `http://www-clued0.fnal.gov/~nunne/cross-sections/mcfm_cross-sections.html`.

[23] N. Kidonakis and R. Vogt, *Theoretical status of the top quark cross section*, Int. J. Mod. Phys. A **20**, 3171 (2005).

[24] T. Andeen *et al.*, *The DØ Experiment's Integrated Luminosity for Tevatron Run IIa*, Fermilab-TM-2365 (2007).

[25] G. Snow (Luminosity Working Group), *Adjustments to the Measured Integrated Luminosity in Run IIa*, DØ Note 5139 (2006).

[26] The Common Sample Group, `http://www-d0.fnal.gov/Run2Physics/cs/index.html`.

[27] The EM-ID Group, `http://www-d0.fnal.gov/phys_id/emid/d0_private/certification/welcome.html`.

[28] Single Electron Triggers – D0Wiki, `https://plone4.fnal.gov/P1/D0Wiki/tdaq/tsg/caftrigger/singleetriggers`

[29] Di-Electron Triggers – D0Wiki, `https://plone4.fnal.gov/P1/D0Wiki/tdaq/tsg/caftrigger/dietriggers`

[30] P. Verdier, private communication (15/09/06).

[31] S.-J. Park and M. Begel, *Efficiency of the Data Quality Calorimeter Flags*, DØ Note 5324 (2007).

[32] U. Blumenschein, *Search for the Associated Production of Chargino and Neutralino in Final States with Two Electrons and an Additional Lepton*, DØ Note 4678 (2005).

[33] A. Ferapontov, private communication.

[34] The Common Analysis Format,
http://www-d0.fnal.gov/Run2Physics/cs/caf.

[35] V. Büscher, J.-F. Grivaz, T. Nunnemann, M. Wobisch, *Conclusions of Mini-Workshop on PDF uncertainties and Related Topics*, DØ Note 4618 (2004).

[36] V. Büscher, J.-F. Grivaz, J. Hobbs *et al.*, *Recommendation of the Ad-Hoc Committee on Limit-Setting Procedures to be Used by DØ in Run II*, DØ Note 4629 (2004).

[37] I. Bertram *et al.* (D0 Collaboration), FERMILAB-TM-2104 (2000);
Simple Limit Calculator, http://www-clued0.fnal.gov/∼hobbs/limit_calc/limit_calc.html.

[38] Heather K. Gerberich, private communication.

[39] Emmanuel Sauvan, private communication.

Table 13: The cut flow for the pre-selection and the final sample.

Cut	DY(ee) + γ	DY(ee) + jet	DY($\tau\tau$)	WW +WZ +ZZ	$t\bar{t}$	QCD	SM Bgrd. Sum	Data	Signal eff. [%] m_{e^*} = 300 GeV	Signal eff. [%] m_{e^*} = 800 GeV
2 EM objects, 2 tracks, $p_T > 15\,\text{GeV}$	69906		390	118	37	—	70452	99726	44.4	49.0
$HMx7/8 < 12/20$	64762		296	105	29	4491	69682	70731	41.7	45.8
$\Delta R > 0.4$	64762		296	105	29	4490	69681	70720	41.6	45.8
no ECN/ECS	64627		296	104	29	4488	69543	70534	41.1	45.6
$p_T(e1) > 25\,\text{GeV}$	58895		199	101	28	2656	61868	62930	41.1	45.6
3^{rd} EMobj ($p_T > 15\,\text{GeV}$) & track veto & CC or EC)	399	129 (MC)	1	4	2	32	567	601	32.9	36.6
emfrac > 0.97	347	72 (MC)	1	3	1	21	445	493	32.9	35.2
isolation < 0.07	288	25 (MC)	1	2	0	9	325	361	31.8	35.1
in-η-fiducial	284	23 (MC)	1	2	0	9	319	357	31.8	34.5
$\Delta R > 0.4$	283	23 (MC)	1	2	0	9	318	357	31.3	34.5
σ_ϕ_EM3 & σ_z_EM3	233	4 (MC)	1	1	0	5	244	259	28.5	33.8
Track isolation	226	7 (scaled)	1	1	0	4	239	259	27.4	32.9

	$m_{e^*} = 200$ GeV	$m_{e^*} = 300$ GeV
Run number	202101	174429
Event number	35629781	13763152
$e1$: p_T, η, ϕ, q	63.7 GeV, -0.800, 3.105, $+$	124.1 GeV, 0.606, -1.334, $-$
$e2$: p_T, η, ϕ, q	46.9 GeV, -1.768, 1.599, $-$	24.8 GeV, 0.128, 3.067, $+$
γ: p_T, η, ϕ	94.1 GeV, 0.199, -0.675	103.1 GeV, -1.073, 1.714
$m(e^*$ candidate)	194.6 GeV	310.6 GeV
$m(e1, e2)$	92.8 GeV	93.6 GeV
$m(e1, \gamma)$	167.8 GeV	310.6 GeV
$m(e2, \gamma)$	194.6 GeV	90.3 GeV
$m(e1, e2, \gamma)$	273.2 GeV	336.8 GeV

Table 14: Details about the two candidate events.